






A common coupling mechanism for A-type heme-copper oxidases from bacteria to mitochondria

Amandine Maréchal^{a,b,1} , Jing-Yang Xu^{b,2} , Naho Genko^b, Andrew M. Hartley^a , Francis Haraux^c, Brigitte Meunier^c , and Peter R. Rich^{b,1} 

^aDepartment of Biological Sciences, Birkbeck College, WC1E 7HX London, United Kingdom; ^bDepartment of Structural and Molecular Biology, University College London, WC1E 6BT London, United Kingdom; and ^cUniversité Paris-Saclay, Commissariat à l'énergie atomique et aux énergies alternatives, CNRS, Institute for Integrative Biology of the Cell (I2BC), 91198 Gif-sur-Yvette, France

Edited by Harry B. Gray, California Institute of Technology, Pasadena, CA, and approved March 16, 2020 (received for review January 27, 2020)

Mitochondria metabolize almost all the oxygen that we consume, reducing it to water by cytochrome *c* oxidase (CcO). CcO maximizes energy capture into the protonmotive force by pumping protons across the mitochondrial inner membrane. Forty years after the H⁺/e⁻ stoichiometry was established, a consensus has yet to be reached on the route taken by pumped protons to traverse CcO's hydrophobic core and on whether bacterial and mitochondrial CcOs operate via the same coupling mechanism. To resolve this, we exploited the unique amenability to mitochondrial DNA mutagenesis of the yeast *Saccharomyces cerevisiae* to introduce single point mutations in the hydrophilic pathways of CcO to test function. From adenosine diphosphate to oxygen ratio measurements on preparations of intact mitochondria, we definitively established that the D-channel, and not the H-channel, is the proton pump of the yeast mitochondrial enzyme, supporting an identical coupling mechanism in all forms of the enzyme.

mitochondria | cytochrome *c* oxidase | H/e stoichiometry | proton pumping | ADP/O ratio

Adenosine triphosphate (ATP) is the universal energy currency of our cells. It is hydrolyzed to fuel energy-requiring biological processes and is continuously resynthesized by condensation of adenosine diphosphate (ADP) and inorganic phosphate (Pi). In humans, roughly our body weight of ATP has to be recycled every day (1). Most of this ATP is produced in mitochondria via oxidative phosphorylation (OXPHOS) in a process that couples the activity of the electron transport chain (ETC) to that of the ATP synthase. OXPHOS is carried out by five major protein complexes embedded in the inner mitochondrial membrane. Complexes I to IV form the ETC responsible for maintenance of the protonmotive force (PMF) that drives ATP synthesis by complex V, the F₁F₀-ATP synthase. Complexes I and II oxidize NADH and succinate, respectively, and pass their electrons via ubiquinone to complex III. Complex III relays the electrons via soluble cytochrome *c* to complex IV (cytochrome *c* oxidase, CcO), which reduces molecular oxygen to water.

Complexes I, III, and IV have evolved mechanisms to maximize the efficiency of capture into the PMF of the energy released by their redox reactions (2, 3). In mitochondrial CcO, the reduction of molecular oxygen to water with four electrons from intermembrane cytochrome *c* and four substrate protons from the matrix conserves part of the available redox energy in the PMF. However, in each full catalytic cycle, four additional protons are transferred across the inner mitochondrial membrane (4), roughly doubling the energy capture efficiency. Substrate and translocated protons must traverse the overall hydrophobic membrane protein along hydrophilic channels formed by appropriate amino acids and associated waters (5, 6), and three possible pathways for this have been identified within available atomic structures (7, 8): the D-, K-, and H-channels. To investigate their contribution to the coupling mechanism, a wide range of spectroscopic, electrometric, mutation and simulation

studies have been performed on bacterial A1-type heme-copper oxidases (HCOs), which are closely related to mitochondrial CcOs (9–11) and have the same catalytic cycle and 1H⁺/e⁻ pumping stoichiometry. The most widely studied of these are the quinol oxidase, cytochrome *bo*₃, from *Escherichia coli* and the *aa*₃ CcOs from *Rhodobacter sphaeroides* and *Paracoccus denitrificans*.

A consensus has been reached on the essential contributions of the K- and D-channels to the oxygen reduction cycle and delivery of the substrate protons to the binuclear center (BNC) (12–15). In addition, it is generally acknowledged that translocated protons that are taken up from the negative aqueous (N) phase of the inner membrane are stored in a transient proton trap before they are expelled into the positive aqueous (P) phase (16). However, there is an ongoing dispute regarding the path into the trap for translocated protons. A diverse body of data on bacterial systems indicates that the D-channel provides a major section of that path (12, 15); however, structural studies and more limited biophysical data on mammalian (bovine) mitochondrial CcO suggest that the translocated protons instead travel into the trap via the H-channel (17).

Here we address this issue using yeast (*Saccharomyces cerevisiae*) mitochondrial CcO. This system has the crucial advantage of facile mtDNA mutagenesis technology that has enabled

Significance

We present a comprehensive investigation of mitochondrial DNA-encoded variants of cytochrome *c* oxidase (CcO) that harbor mutations within their core catalytic subunit I, designed to interrogate the presently disputed functions of the three putative proton channels. We assess overall respiratory competence, specific CcO catalytic activity, and, most importantly, proton/electron (H⁺/e⁻) stoichiometry from adenosine diphosphate to oxygen ratio measurements on preparations of intact mitochondria. We unequivocally show that yeast mitochondrial CcO uses the D-channel to translocate protons across its hydrophilic core, providing direct evidence in support of a common proton pumping mechanism across all members of the A-type heme-copper oxidase superfamily, independent of their bacterial or mitochondrial origin.

Author contributions: A.M. and P.R.R. designed research; A.M., J.-Y.X., N.G., A.M.H., F.H., and B.M. performed research; A.M. analyzed data; and A.M. and P.R.R. wrote the paper. The authors declare no competing interest.

This article is a PNAS Direct Submission.

This open access article is distributed under [Creative Commons Attribution-NonCommercial-NoDerivatives License 4.0 \(CC BY-NC-ND\)](https://creativecommons.org/licenses/by-nc-nd/4.0/).

¹To whom correspondence may be addressed. Email: a.marechal@ucl.ac.uk or prr@ucl.ac.uk.

²Present address: Department of Laboratory Medicine and Pathology, University of Alberta, Edmonton, AB, Canada T6G 2G3.

This article contains supporting information online at <https://www.pnas.org/lookup/suppl/doi:10.1073/pnas.2001572117/-DCSupplemental>.

First published April 14, 2020.

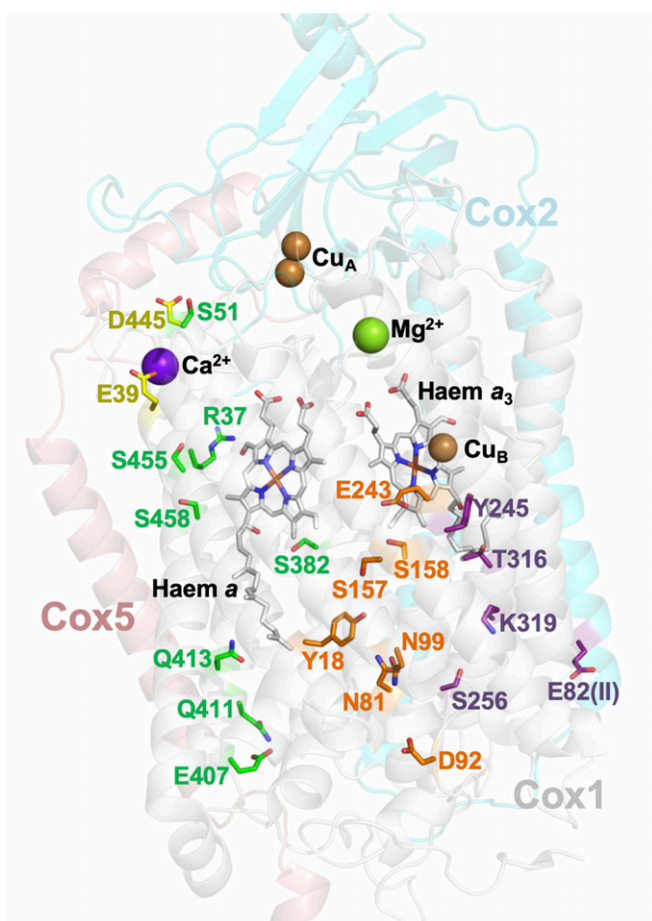


Fig. 1. The three possible proton-conducting channels of yeast CcO. The residues forming the H-, D-, and K-channels are colored in green, orange, and purple, respectively. D445E and E39Q, which are not located in the proton channels, are displayed in yellow. Atomic coordinates were taken from Protein Data Bank ID code 6HU9 (18).

the mutation of residues of mtDNA-encoded subunit I (Cox1) located in the D-, K-, and H-channels. Mutations in the D- and H-channels were originally described by Meunier et al. (19), with sites chosen from a three-dimensional (3D) model of the yeast enzyme built by sequence homology onto the bovine enzyme crystal structure (20). The positions of all mutations used in the present study were recently confirmed in the atomic resolution structure of the yeast CcO (18) (Fig. 1). Here we show that effects of mutations in all three channels on catalytic turnover and coupled proton transfer closely mirror the effects of equivalent mutations in the closely related bacterial oxidases, supporting a common coupling mechanism in all members of the A1-type branch of HCOs independent of their bacterial or mitochondrial origin.

Results

Mutations in the D- and the K-Channels Are Detrimental to Respiratory Growth, but Those in the H-Channel Are Not. All yeast strains were derived from W303-1B (WT) which was modified to express CcO with a 6-histidine tag at the C terminus of its Cox13 subunit (6H-WT), as described by Meunier et al. (19). Subsequently, variants of 6H-WT were constructed harboring point mutations in the three putative proton pathways within Cox1: N99D, E243D, and I67N in the D-channel; Q411L, Q413L, S382A, S458A, S455A, and S52D in the H-channel; and T316K in the K-channel (Fig. 1). Two other mutant strains were also

included in this study: D445E, previously identified by random mutagenesis to be respiratory-deficient (21), and E39Q, which contributes to the $\text{Na}^+/\text{Ca}^{2+}$ -binding site near the top of the H-channel (both displayed in yellow in Fig. 1). All mutant strains presented here successfully assembled CcO (SI Appendix, Fig. S1).

The effect of the mutations was first assessed on whole-cell doubling times when cultured in a medium with the respiratory substrate glycerol (Fig. 2). The doubling times of the six H-channel mutants were not significantly different from those of the WT or 6H-WT strain (mean, 3.6 ± 0.4 h for the 6H-WT strain). This contrasts with the D- and K-channel mutants, all of which showed longer doubling times, ranging from mild (N99D, 5.4 ± 0.9 h) to severe (I67N and T316K, 196.1 ± 78.4 and 40.5 ± 4.7 h, respectively) respiratory growth impairment. Mutant D445E (15.9 ± 1.8 h) showed a pronounced respiratory impairment, while E39Q grew with a doubling time similar to WT.

Mutations in the D- and K-Channels, but Not Those in the H-Channel, Severely Affect Catalytic Turnover. Yeast strains were grown aerobically on galactose and mitochondrial membrane fragments were prepared from cells harvested in log phase (19) (Materials and Methods). Turnover numbers (TNs) for each CcO variant were determined from oxygen consumption rates at pH 6.6 in the presence of N,N,N',N' -tetramethyl-p-phenylenediamine (TMPD), ascorbate, and cytochrome c (Fig. 3 and SI Appendix, Table S1). All H-channel mutants and E39Q displayed a TN similar to that of WT ($1175 \pm 161 \text{ e}\cdot\text{s}^{-1}$). Significantly different TNs were measured for the three D-channel variants, with reduced rates for I67N and E243D (1% and 46% of the WT value, respectively) but an enhanced rate for N99D (151% of the WT value). The K-channel mutant T316K also had a low TN (15% of WT) as did the D445E mutant (44% of WT).

ADP/O Ratios: Theoretical Values. ADP/O ratios (and hence H^+/e^- ratios) were determined with ADP pulses given to intact isolated mitochondria respiring with a respiratory substrate for all variants except I67N, whose TN is too low to allow measurement. Several substrates were tested, including NADH, succinate, and ethanol (SI Appendix, Table S2), but the highest respiratory

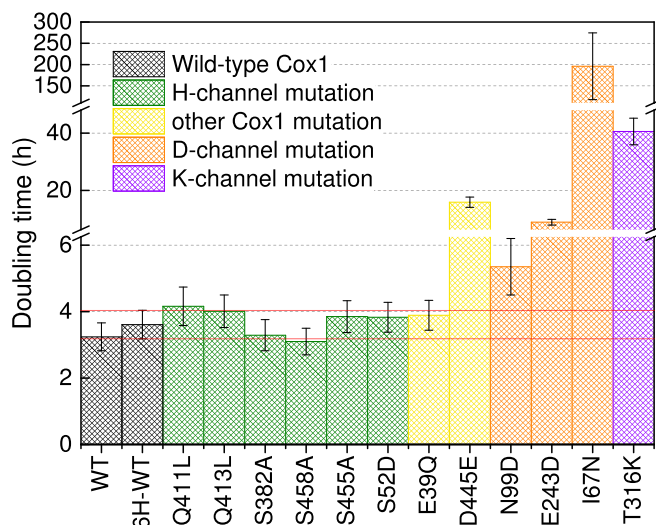


Fig. 2. Doubling times of yeast strains cultured in glycerol medium. The strains harbor mutations in the H- (green), D- (orange), or K-channel (purple), the three putative proton transfer pathways in Cox1, or mutations E39Q and D445E. Also included for comparison are the WT yeast strain and the WT with an additional 6-histidine tag at the C terminus of the nuclear encoded subunit Cox13 (6H-WT), both displayed in black.

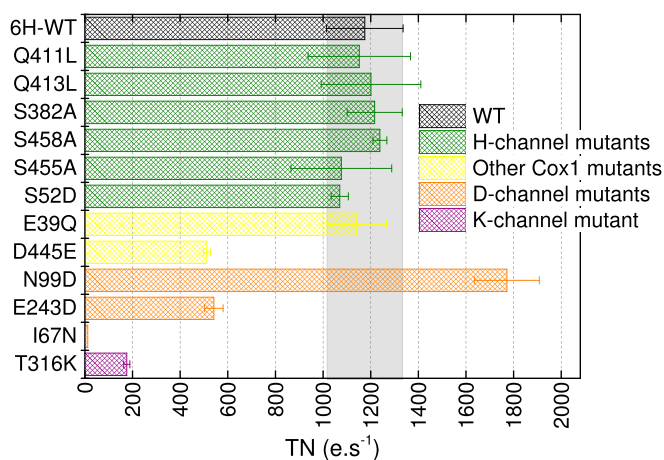


Fig. 3. TNs of CcO in mitochondrial membranes. TNs were measured from oxygen consumption rates at pH 6.6 in the presence of ascorbate, TMPD, and cytochrome c and are expressed as electrons per second (e.s⁻¹) per CcO.

coupling ratios (RCRs; ratio of state 3/state 4 respiratory rates) (22), and therefore the most accurate H⁺/e⁻ ratios (see below), were obtained with α -ketoglutarate. This is because α -ketoglutarate is oxidized only by intact mitochondria (23) and because of the direct kinetic control exerted by the ADP/ATP ratio on α -ketoglutarate dehydrogenase (24).

α -Ketoglutarate is imported into mitochondria via a specific carrier that exchanges it for malate. Once inside the mitochondrion, α -ketoglutarate enters the Krebs cycle, where it is converted to succinyl CoA by α -ketoglutarate dehydrogenase, producing one equivalent of NADH. Succinyl CoA is transformed into succinate by succinyl thiokinase, producing one ATP equivalent. Succinate is then oxidized to fumarate by complex II, and fumarate is converted to malate, which is transported out of the mitochondrion in exchange for another α -ketoglutarate. In *S. cerevisiae* mitochondria, both succinate and NADH reduce ubiquinone with nonprotonmotive enzymes (25). For every two electrons from reduced ubiquinone passing through complexes III and IV to reduce 1/2 O₂ to H₂O, six protons are translocated across the membrane. Thus, since succinate and NADH together provide four electrons to the ETC, reducing O₂ into 2 H₂O, this results in the translocation of 12 H⁺ from the matrix to the intermembrane space (IMS) and the formation of one matrix-located ATP. As one H⁺ is used to export this substrate-level

ATP out of the matrix, one α -ketoglutarate results in 11 H⁺ overall and one ATP translocated from the matrix to the IMS. The yeast *S. cerevisiae* F₁F₀-ATPase has 10 c-subunits (26), so 10 H⁺ are required to produce three molecules of matrix ATP, and three additional H⁺ are required to translocate them into the IMS, i.e., 13 H⁺ for three ATP_{cytoplasmic}. Thus, when one α -ketoglutarate is oxidized to malate, two O (one O₂) are reduced, and the total ATP produced outside the matrix is $1_{\text{substrate level-ATP}} + 11/(13/3)_{\text{OXPHOS-ATP}} = 3.54$, giving an ADP/O ratio of $3.54/2 = 1.77$ (of which 1.27 ATP arise from OXPHOS and 0.5 ATP arises from substrate-level phosphorylation). If the proton translocation activity of CcO becomes uncoupled from its oxygen-reducing cycle (i.e., oxygen reduction and proton uptake to form water occur but no additional protons are translocated), then the oxidation of α -ketoglutarate to malate results in only eight proton translocations (four from succinate and four from NADH), decreasing the ADP/O ratio to $(1_{\text{substrate level-ATP}} + 7/(13/3)_{\text{OXPHOS-ATP}})/2 = 1.31$, of which 0.81 ATP now arises from OXPHOS and 0.5 ATP is still produced from substrate-level phosphorylation.

Mutation in the Yeast Mitochondrial CcO D-Channel, but Not in the H- or K-Channel, Results in Loss of Coupled Proton Translocation. With α -ketoglutarate as a substrate, RCRs following small additions of ADP ranged from 1.6 to 2.4 in different preparations of intact mitochondria (*SI Appendix, Table S1*). ADP/O ratios were calculated from the additional oxygen consumption induced by ADP conversion to ATP under the assumption that 50% of state 4 oxygen consumption rate continues in state 3, as described in *Materials and Methods*. In this case, the measured ADP/O ratio of 6H-WT mitochondria was 1.73 ± 0.15 (Fig. 4A and B), which is close to the theoretical value of 1.77 for a fully coupled respiratory chain, giving an H⁺/e⁻ pumping stoichiometry of 0.9 ± 0.3 for CcO (see above). All H-channel mutants and K-channel mutant T316K displayed ADP/O ratios similar to that of the 6H-WT (Fig. 4B), as did E39Q and D445E, ruling out any essential involvement of these residues in proton translocation. In contrast, mutations in the D-channel gave significantly different ADP/O ratios. E243D displayed a higher value, at 2.18 ± 0.10 (Fig. 4B). The most reasonable explanation for this finding is that <50% of the state 4 rate persists in state 3 in this mutant, with no change to the H⁺/e⁻ stoichiometry of CcO. However, mutant N99D displayed an ADP/O ratio of 1.39 ± 0.09 (Fig. 4A and B), consistent with a loss of the coupled proton translocation associated with the CcO oxygen reduction cycle.

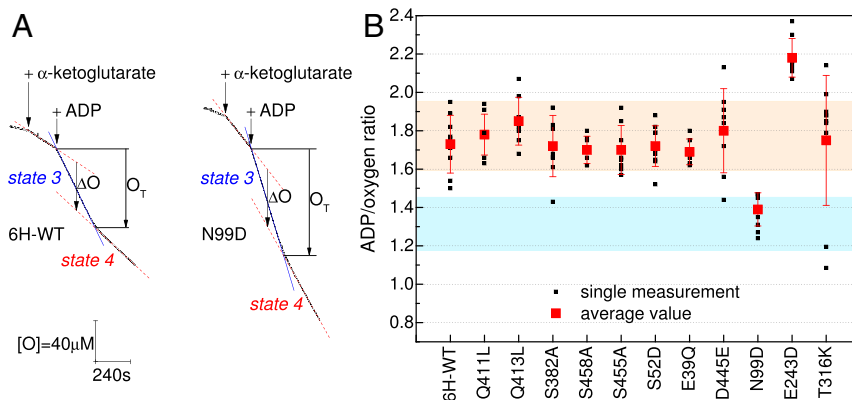


Fig. 4. ADP/O ratio measurements on preparations of intact mitochondria. (A) Oxygen consumption rates of intact yeast mitochondria respiring on α -ketoglutarate. (B) Calculated ADP/O ratios during state 3 respiration. Theoretical ADP/O values for respiration on α -ketoglutarate are $1.77 (\pm 10\%)$ (orange band) and $1.31 (\pm 10\%)$ (blue band) depending on whether the CcO additional proton translocation is fully coupled (H⁺/e⁻ ratio of 1.0 ± 0.4) or uncoupled (H⁺/e⁻ ratio of 0.0 ± 0.3), respectively.

Discussion

The mechanism by which mitochondrial CcOs, along with their bacterial homologs in the A1 branch of the HCO superfamily, maximize the energy conservation of the oxygen reduction reaction by translocating protons across the membrane remains a matter of debate (14, 15, 17). A key molecular aspect of this coupling mechanism is the identification of the paths within the protein structure that enable proton transfer, both from the N phase into the BNC for substrate protons and from the N phase into and out of a proton trap for the translocated protons. Three possible pathways—the D-, K-, and H-channels (Fig. 1)—have been identified in the atomic structures of the central catalytic subunit I of both bacterial and mitochondrial CcOs (7, 8).

The ability to mutate the mtDNA-encoded subunit I of yeast CcO provides a means to further explore channel mutation effects and reconcile the body of data from CcOs of mammalian and bacterial origins (*SI Appendix, Table S3*). A range of random and site-directed mutations relevant to channel functions have been reported previously (19, 21, 27–30), several of which have been analyzed further here.

Inhibitory Mutations in the K-, D-, and H-Channels. Several mutations in bacterial oxidases have been shown to severely impair overall catalysis (12, 31–33). Mutation effects on specific component reactions have led to the conclusion that the K-channel conducts substrate protons into the BNC, but only during the two reductive steps before oxygen binds (the O→E→R steps) (15, 34) and/or may act as a “dielectric channel” to facilitate one or both of these steps (35). The D-channel provides the substrate proton route into the BNC for the remaining reductive steps (the P→F and F→O steps) after O-O bond cleavage (14, 15, 36).

In contrast, mutations within the bacterial H-channel (also referred to as the E-channel) did not generally have a marked effect on overall catalysis (37), with two exceptions. Mutation of conserved R52 to A or Q in *R. sphaeroides* (31, 37) did cause inhibition of catalysis but was linked to the disruption of its stabilizing interaction with the heme *a* formyl (37). Replacement of the equivalent residue in yeast with a methionine (R37M) was also linked to an assembly defect (19). Potentially more significant is a report of dramatically decreased catalytic activity in mutant H448L of *P. denitrificans* CcO, a residue located in the lower part of the H-channel (equivalent to H413 in bovine CcO; *SI Appendix, Table S3*). However, this loss appears to have arisen from a severe decrease in heme *a* incorporation rather than from an effect on coupled proton transfer (31). Furthermore, substitution of the equivalent H456 with a smaller alanine in *R. sphaeroides* CcO had no effect on TN or enzyme assembly (37).

In *S. cerevisiae*, D-channel mutants I67N and E243D and K-channel mutant T316K all resulted in longer doubling times of growth on respiratory substrate (>10-, 4- to 5-, and >10-fold, respectively). Consistent with this, their TNs in isolated mitochondria were 1%, 46%, and 15%, respectively. The inhibitory effects of T316K and E243D are consistent with observations in variants of the equivalent T359 of *R. sphaeroides* (38, 39), as well as with E/D replacement of the residue equivalent to E243 in *E. coli* (40), *P. denitrificans* (31), and *R. sphaeroides* (41). We previously showed that yeast mutant I67N (42), for which no equivalent bacterial mutant has been studied, is likely to interfere directly with E243 function at the top of the D-channel (43, 44) and to compromise substrate proton uptake (45, 46). These effects clearly confirm the expected essential roles of the D- and K-pathways in catalysis.

In contrast to these mutants, none of the yeast CcO H-channel mutants tested here significantly affected cell growth or catalytic TNs, consistent with behavior of both bacterial (31, 37) and bovine (47, 48) CcO H-channel mutations.

Uncoupling Mutations. In all three bacterial A1-type HCOs, mutation of some specific asparagine and aspartic acid residues within the D-channel resulted in loss of coupled proton translocation associated with the remaining catalytic turnover. The first report of this was a D135N mutant of cytochrome *bo3* (40, 49), which led to a complete loss of the proton pump accompanied with a decrease of TN to 45% of WT activity. A similar phenotype was reported for equivalent CcO variants D132N of *R. sphaeroides* (38) and D124N of *P. denitrificans* (31), although with a much more dramatic effect on their TNs (4% and 5% of WT activity, respectively). Slightly higher up in the D-channel, mutation N131D in *P. denitrificans* CcO had an ideal uncoupled phenotype (50) with complete loss of proton pumping while retaining close to 100% of the WT O₂-reduction activity. The equivalent CcO variant N139D in *R. sphaeroides* also resulted in uncoupling of proton pumping, while having an increased catalytic activity of 150% to 300% of that of WT with unperturbed catalytic intermediates (51). Facing N131, mutation N199D of *P. denitrificans* CcO, and its N207D equivalent in *R. sphaeroides*, was also shown to uncouple the enzyme, with 45% of and close to WT activity, respectively (50, 52). Interestingly, double mutants of two of these loci (D132N/N139D in *R. sphaeroides*) restored full proton pumping capability (53, 54).

Despite these inconsistencies in effects among the three enzymes (and the fact that measurements were done in different ways on whole cells and purified enzyme reconstituted into vesicles and with pH-electrode vs. stopped-flow spectroscopy) (31, 50, 55), a consensus has been reached that these uncoupling effects arise from the dual role of the D-channel in providing the pathway for both translocated and substrate protons from the matrix (or cytoplasm), with *pK* changes caused by uncoupling mutations within the channel disrupting the necessary controlled distribution of protons between these pathways.

Equivalent D-channel mutations in a mitochondrial system have not been published previously. Instead, three uncoupling variants have been reported in a chimeric human/bovine system, all within the H-channel. These include the single variants D51N and S441P at the top of the H-channel and the double variant M390W/V386L in its lower part below heme *a* (47, 48). Normal electron transfer rates have been reported for all three variants, as would be expected for ideally uncoupled oxidases. These data, together with redox- and ligand-induced structural changes in two domains of the H-channel (56–59), have led to the proposal that it is the H-channel that provides the route for pumped protons both into and out of the proton trap. However, mutagenesis of H-channel residues of bacterial HCOs failed to support any crucial H-channel function. The sole bacterial H-channel mutation for which a loss of pump has been reported is H448L of *P. denitrificans* (31). As noted above, this phenotype has been called into question because of the associated dramatic TN inhibition (5% of WT) and severe defect of heme *a* assembly.

In terms of the effects of the yeast channel mutations on coupling efficiencies, D-channel mutant E243D, K-channel mutant T316K, or any of the H-channel mutants did not result in uncoupling of proton translocation from catalytic turnover. However, importantly and uniquely, of all the mutants tested, D-channel mutant N99D stimulated catalytic turnover (1.5-fold increase) while becoming uncoupled (H⁺/e⁻ stoichiometry of 0.2 ± 0.2) from proton translocation. This mutation also caused a moderate (1.5-fold) increase in cell doubling time, presumably resulting from the uncoupling effect. Mutation N99D in yeast is equivalent to the ideally uncoupled variants N131D of *P. denitrificans* and N139D of *R. sphaeroides* described above, demonstrating that the effect is common to both bacterial and mitochondrial enzymes. Thus, overall, the yeast mutant data clearly point to the same roles of the K- and D-channels in delivery of substrate and pumped protons as occur in homologous

A1-type bacterial oxidases and argue against a role of the H-channel in channeling of protons from the N phase into the proton trap.

Given the similarity of structures in yeast and mammalian CcOs, it seems unlikely that the channel roles have evolved differently in mammalian CcOs. Nevertheless, some structural differences should be acknowledged. For example, in the lower section of the H-channel, a histidine residue is conserved in bovine (H413), *R. sphaeroides* (H456), and *P. denitrificans* (H448) CcOs; however, in yeast CcO, this is replaced by a glutamine (Q413). Mutation of this residue to leucine had no effect on respiratory growth competence, catalytic turnover, or coupling efficiency. In a parallel study (60), further mutations at this site also had negligible effects on respiratory growth competence or catalysis, and molecular dynamics simulations predicted that this span is incapable of protonic conductivity. Molecular dynamics simulations of the same region of bovine CcO also failed to support protonic conductivity of this span unless the histidine can form its imidazolium state, which is considered unlikely due to its low predicted pK_a value (61).

Although the D-channel route into the proton trap is most likely as described above, the path from the trap into the P phase remains generally unresolved. The likely proton trap region is “above” the BNC and close to the bound Mg^{2+}/Mn^{2+} site (16, 62). Protonic connectivity between the trap and P phase may be made through the relatively hydrated “top” region of the H-channel, possibly linked via the conserved pair of arginine ligands to the heme *a* propionates. Several specific routes have been suggested from structures or simulations of bacterial (63, 64) and bovine (16, 65) CcOs. Although some amino acids in this region are not well conserved among mammalian, yeast, and bacterial CcOs (*SI Appendix, Table S3*), the hydrated domains are structurally similar and extensive. Thus, for all CcOs, this top region of the H-channel may provide a hydrated H-bonded network with several facile proton pathways into the P phase.

Yeast Mutants D445E and E39Q Do Not Affect Proton Coupling. Apart from the K- and D-channel variants described above, only mutation of D445E was found to impair catalytic TN (44% of WT), again with direct repercussion on respiratory growth competence with a cell doubling time greater than fourfold longer than that of WT. D445 is at the top of helix XI, in a region above the proposed calcium-binding site at the interface of Cox1, Cox5a, and Cox2 (18) and within H-bonding distance of T123 and M124 of Cox5a and the main chain amide of R159 of Cox2. From Fourier-transform infrared spectroscopy studies, R159 has been implicated in Ca^{2+}/Na^+ binding via the salt bridge formed by its guanidinium with D442 of Cox1 (66). Replacement of D445 with the longer side chain glutamic acid most likely disrupts these interactions. Such disruption could impact biogenesis, which starts with the assembly of a Cox1-Cox5 module before association with Cox2 (67). Indeed, the low level of observable heme *a* in this variant is ~20% that in WT cells (at 0.4 nmol CcO/g wet weight of cells and a correspondingly low heme *a/bc_1* complex ratio in mitochondria), which could be caused by an assembly defect or possibly poor heme *a* incorporation. Misfolding of this region could also alter the presentation of residues at the surface, with effects on cytochrome *c* docking and electron transfer to the dinuclear Cu_A center.

In contrast, mutation E39Q, a residue directly involved in calcium binding, had no effect on TN or cell growth, consistent with studies on the equivalent bacterial variant (68). Importantly, neither D445E nor E39Q had an effect on the extent of coupled proton transfer. Thus, despite being potentially linked into the extensive hydrated top region of the H-channel, neither residue can have an essential function in the proton exit route from the trap into the P phase.

In summary, whether the H-channel can play a role in modulating catalysis or whether its top domain can provide an exit route for protons from trap into the P phase remains to be investigated. The present work has definitely established that, as for equivalent bacterial systems, the D-channel is the lower part of the pumping element for proton translocation in yeast mitochondrial CcO.

Materials and Methods

Yeast extract was purchased from Ohly. All chemicals were purchased from Sigma-Aldrich unless specified otherwise.

Construction of Yeast Mutants. Of the 12 mutants studied, three (I67N, T316K, and D445E) were obtained by random mutagenesis as first described by Meunier et al. (27) and the other nine were constructed by site-directed mutagenesis following a previously described method (69, 70). The mutations were transferred by cytoduction (71) into a strain derived from W303-1B (72) that carries a 6-histidine tag sequence on the 3' end of nuclear gene *COX13* (19). 6H-WT and all mutants have identical nuclear and mitochondrial genomes, except for the point mutations in *COX1*. Strains WT and 6H-WT differ only by the 6-histidine tag on *COX13*.

Yeast Culture on Respiratory Medium. Yeast cells were grown at 28 °C in respiratory YPGly medium (1% yeast extract, 2% peptone, 2% glycerol) in two parallel flasks, with the second flask inoculated 8 h after the first flask. Every 2 h a sample was taken in each flask under aseptic conditions, and the OD_{600} value was measured, interpolating sampling times of the second flask to best cover the complete time range of growth. The doubling time for each strain was derived from a fit to the linear region of \log_{10} -vs.-time plots using OriginPro (OriginLab), and the error displayed is the SE of the fit.

Catalytic TNs. TNs for each mutant strain were determined in mitochondrial membrane fragments prepared from cells cultured in YPGal medium (1% yeast extract, 2% peptone, 2% galactose), as described by Meunier et al. (19), by measurement of steady-state oxygen consumption rates at 25 °C with a Clark-type oxygen electrode (Oxygraph; Hansatech). Assays were conducted in a medium of 10 mM KPi and 50 mM KCl at pH 6.6 and containing 0.05% *n*-dodecyl- β -D-maltoside, 40 μ M TMPD, and 50 μ M horse heart cytochrome *c*. After equilibration and recording of the basal rate, the reaction was initiated by the addition of 2 mM Na^+ -ascorbate. TNs were calculated as $e.s^{-1}.CcO^{-1}$ from a fit to the linear region of the oxygen consumption rate using Origin (OriginLab). Results are the average (\pm SD) of *n* independent experiments from at least two independent mitochondrial preparations.

Preparation of Intact Mitochondria. Intact mitochondria were prepared from 12 to 15 g of yeast cells (wet weight) grown aerobically at 28 °C in YPGal medium (1% yeast extract, 2% peptone, 2% galactose) and harvested in log phase. The digestion of the yeast cell wall was performed enzymatically following a modified version of the protocol described by Guérin et al. (73). First, cells were incubated for 10 min at 32 °C with 20 mL per g of wet weight of cells of a solution containing 0.1 M Tris-HCl and 0.5 M β -mercaptoethanol at pH 9.3. Cells were then pelleted for 5 min at 2,500 \times g and 4 °C, after which the supernatant was discarded. The cell pellet was washed twice by resuspension/centrifugation (5 min at 2,500 \times g) cycles performed at 4 °C with 500 mL of 10 mM Tris-HCl and 0.5 M KCl at pH 7. The final pellet of cells was resuspended in a solution containing 1.35 M sorbitol, 1 mM EGTA, 10 mM citric acid, and 30 mM sodium phosphate at pH 5.8 at a volume of 10 mL per g of wet weight of cells. Zymolyase (MP Biomedicals) was added to the cell suspension at a concentration of 10 mg per g of wet weight of cells, and the mixture was incubated in a water bath at 32 °C, with occasional mixing, for 60 to 90 min. Spheroplast formation was followed by visual inspection under a light microscope of aliquots of the cell suspension diluted by a factor of 2 with water. Once digestion was complete, the spheroplast suspension was centrifuged for 5 min at 4,000 \times g and 4 °C, and the supernatant was removed. The spheroplast pellet was washed twice by resuspension/centrifugation (5 min at 2,500 \times g, 4 °C) cycles performed at 4 °C with 200 mL of a solution containing 0.75 M sorbitol, 0.4 M mannitol, 0.1% BSA (w:v), and 10 mM Tris-maleate at pH 6.8. The resulting pellet was resuspended with a solution of 0.5 M mannitol, 0.2% BSA (w:v), 2 mM EGTA, and 10 mM Tris-maleate at pH 6.8 and then transferred to a Potter–Elvehjem homogenizer with a Teflon pestle, where spheroplast lysis was achieved both osmotically and mechanically. The suspension was centrifuged for 10 min at 800 \times g and 4 °C, and the pellet was discarded. The supernatant was distributed among six centrifuge tubes and centrifuged for 10 min at

12,000 × *g* and 4 °C. The resulting mitochondrial pellets were resuspended in a small volume of solution containing 0.6 M mannitol, 2 mM EGTA, and 10 mM Tris-maleate at pH 6.8 (buffer A) and gently homogenized with the Potter pestle, and the centrifuged tubes were refilled again with buffer A. Following a low-speed centrifugation (5 min at 800 × *g* and 4 °C) with elimination of the resulting pellets, the supernatants were centrifuged for 10 min at 12,000 × *g* and 4 °C. The pellets obtained were washed once more with buffer A, following the above steps of homogenization, low-speed centrifugation, and high-speed centrifugation. The final pellet of mitochondria was resuspended with the smallest amount of buffer A and gently homogenized with a small Potter–Elvehjem homogenizer, and ADP/O ratios were measured immediately.

ADP/O Ratio Measurements. ADP/O measurements were performed with the oxygen-electrode setup described above in a medium of 0.65 M mannitol, 5 mM MgCl₂, 3 mM KPI, 10 mM Tris-maleate, 17 mM KCl, and 0.1% BSA (w:v) at pH 7.0 and 25 °C. Oxygen consumption rates were determined after successive additions of intact mitochondria (10 to 20 μL), 10 mM α-ketoglutarate (Na⁺ salt), and 100 μM ADP (Na⁺ salt). The latter induced state 3 of respiration, which spontaneously reverted to state 4 after all the ADP was transformed into ATP. The RCR was calculated from the ratio of the state 3 to state 4 oxygen consumption rates measured. The ADP/O values

presented here are the average of the ADP/O_T and ADP/ΔO values determined after ADP addition; error bars represent the SD from the mean. O_T, representing the total oxygen consumed during state 3 assuming no state 4 in state 3, was determined graphically from the difference in oxygen concentrations between the onset of state 3 and the intersection of the two straight lines extrapolating state 3 and state 4. ΔO represents the oxygen consumed during state 3 assuming that state 4 occurs also in state 3. ΔO was determined graphically from the difference in oxygen concentration between the two straight lines extrapolated from the linear regimes of oxygen consumption before ADP addition and after stabilization of state 4, measured at the point at which one-half of the O_T had been consumed.

Data Availability. All relevant data are included in the paper and are available from the corresponding author upon reasonable request.

ACKNOWLEDGMENTS. This work was supported by the Medical Research Council UK (Career Development Award MR/M00936X/1, to A.M.); the European Cooperation in Science and Technology (COST) action CM1306, with short-term scientific visit awards to A.M., B.M., and F.H.; and the UK Biotechnology and Biological Sciences Research Council (Awards BB/K001094/1 and BB/L020165/1, to P.R.R.).

1. P. Rich, Chemiosmotic coupling: The cost of living. *Nature* **421**, 583 (2003).
2. P. R. Rich, A. Maréchal, "Electron transfer chains: Structures, mechanisms and energy coupling" in *Comprehensive Biophysics*, S. J. Ferguson, Ed. (Elsevier, 2012), pp. 72–93.
3. M. Wikström, V. Sharma, V. R. I. Kaila, J. P. Hosler, G. Hummer, New perspectives on proton pumping in cellular respiration. *Chem. Rev.* **115**, 2196–2221 (2015).
4. M. K. F. Wikström, Proton pump coupled to cytochrome *c* oxidase in mitochondria. *Nature* **266**, 271–273 (1977).
5. J. F. Nagle, S. Tristram-Nagle, Hydrogen-bonded chain mechanisms for proton conduction and proton pumping. *J. Membr. Biol.* **74**, 1–14 (1983).
6. T. E. Decoursey, Voltage-gated proton channels and other proton transfer pathways. *Physiol. Rev.* **83**, 475–579 (2003).
7. S. Iwata, C. Ostermeier, B. Ludwig, H. Michel, Structure at 2.8 Å resolution of cytochrome *c* oxidase from *Paracoccus denitrificans*. *Nature* **376**, 660–669 (1995).
8. T. Tsukihara *et al.*, The whole structure of the 13-subunit oxidized cytochrome *c* oxidase at 2.8 Å. *Science* **272**, 1136–1144 (1996).
9. J. A. García-Horsman, B. Barquera, J. Rumbley, J. Ma, R. B. Gennis, The superfamily of heme-copper respiratory oxidases. *J. Bacteriol.* **176**, 5587–5600 (1994).
10. F. L. Sousa *et al.*, The superfamily of heme-copper oxygen reductases: Types and evolutionary considerations. *Biochim. Biophys. Acta* **1817**, 629–637 (2012).
11. J. Hemp, R. B. Gennis, "Diversity of the heme-copper superfamily in archaea: Insights from genomics and structural modeling" in *Bioenergetics. Results and Problems in Cell Differentiation*, G. Schäfer, H. S. Penefsky, Eds. (Springer, 2008), pp. 1–31.
12. P. Brzezinski, R. B. Gennis, Cytochrome *c* oxidase: Exciting progress and remaining mysteries. *J. Bioenerg. Biomembr.* **40**, 521–531 (2008).
13. P. R. Rich, A. Maréchal, Functions of the hydrophilic channels in protonmotive cytochrome *c* oxidase. *J. R. Soc. Interface* **10**, 20130183 (2013).
14. P. R. Rich, Mitochondrial cytochrome *c* oxidase: Catalysis, coupling and controversies. *Biochem. Soc. Trans.* **45**, 813–829 (2017).
15. M. Wikström, K. Krab, V. Sharma, Oxygen activation and energy conservation by cytochrome *c* oxidase. *Chem. Rev.* **118**, 2469–2490 (2018).
16. N. Yano *et al.*, The Mg²⁺-containing water cluster of mammalian cytochrome *c* oxidase collects four pumping proton equivalents in each catalytic cycle. *J. Biol. Chem.* **291**, 23882–23894 (2016).
17. S. Yoshikawa, A. Shimada, Reaction mechanism of cytochrome *c* oxidase. *Chem. Rev.* **115**, 1936–1989 (2015).
18. A. M. Hartley *et al.*, Structure of yeast cytochrome *c* oxidase in a supercomplex with cytochrome *bc*₁. *Nat. Struct. Mol. Biol.* **26**, 78–83 (2019).
19. B. Meunier, A. Maréchal, P. R. Rich, Construction of histidine-tagged yeast mitochondrial cytochrome *c* oxidase for facile purification of mutant forms. *Biochem. J.* **444**, 199–204 (2012).
20. A. Maréchal, B. Meunier, D. Lee, C. Orengo, P. R. Rich, Yeast cytochrome *c* oxidase: A model system to study mitochondrial forms of the haem-copper oxidase superfamily. *Biochim. Biophys. Acta* **1817**, 620–628 (2012).
21. B. Meunier, P. R. Rich, Second-site reversion analysis is not a reliable method to determine distances in membrane proteins: An assessment using mutations in yeast cytochrome *c* oxidase subunits I and II. *J. Mol. Biol.* **283**, 727–730 (1998).
22. B. Chance, G. R. Williams, Respiratory enzymes in oxidative phosphorylation, III: The steady state. *J. Biol. Chem.* **217**, 409–427 (1955).
23. C. M. Smith, J. Bryla, J. R. Williamson, Regulation of mitochondrial alpha-ketoglutarate metabolism by product inhibition at alpha-ketoglutarate dehydrogenase. *J. Biol. Chem.* **249**, 1497–1505 (1974).
24. J. G. McCormack, R. M. Denton, The effects of calcium ions and adenine nucleotides on the activity of pig heart 2-oxoglutarate dehydrogenase complex. *Biochem. J.* **180**, 533–544 (1979).
25. J. P. Lasserre *et al.*, Yeast as a system for modeling mitochondrial disease mechanisms and discovering therapies. *Dis. Model. Mech.* **8**, 509–526 (2015).
26. D. Stock, A. G. W. Leslie, J. E. Walker, Molecular architecture of the rotary motor in ATP synthase. *Science* **286**, 1700–1705 (1999).
27. B. Meunier, P. Lemarre, A. M. Colson, Genetic screening in *Saccharomyces cerevisiae* for large numbers of mitochondrial point mutations which affect structure and function of catalytic subunits of cytochrome-*c* oxidase. *Eur. J. Biochem.* **213**, 129–135 (1993).
28. S. Brown, A. M. Colson, B. Meunier, P. R. Rich, Rapid screening of cytochromes of respiratory mutants of *Saccharomyces cerevisiae*. Application to the selection of strains containing novel forms of cytochrome-*c* oxidase. *Eur. J. Biochem.* **213**, 137–145 (1993).
29. B. Meunier, A. M. Colson, Random deficiency mutations and reversions in the cytochrome *c* oxidase subunits I, II and III of *Saccharomyces cerevisiae*. *Biochim. Biophys. Acta* **1187**, 112–115 (1994).
30. C. Ortwein *et al.*, Structural and functional analysis of deficient mutants in subunit I of cytochrome *c* oxidase from *Saccharomyces cerevisiae*. *Biochim. Biophys. Acta* **1321**, 79–92 (1997).
31. U. Pflitzner *et al.*, Cytochrome *c* oxidase (heme *aa*₃) from *Paracoccus denitrificans*: Analysis of mutations in putative proton channels of subunit I. *J. Bioenerg. Biomembr.* **30**, 89–97 (1998).
32. M. Wikström, Cytochrome *c* oxidase: 25 years of the elusive proton pump. *Biochim. Biophys. Acta* **1655**, 241–247 (2004).
33. J. P. Hosler, S. Ferguson-Miller, D. A. Mills, Energy transduction: Proton transfer through the respiratory complexes. *Annu. Rev. Biochem.* **75**, 165–187 (2006).
34. A. A. Konstantinov, S. Siletsky, D. Mitchell, A. Kaulen, R. B. Gennis, The roles of the two proton input channels in cytochrome *c* oxidase from *Rhodobacter sphaeroides* probed by the effects of site-directed mutations on time-resolved electrogenic intraprotein proton transfer. *Proc. Natl. Acad. Sci. U.S.A.* **94**, 9085–9090 (1997).
35. S. Jünemann, B. Meunier, R. B. Gennis, P. R. Rich, Effects of mutation of the conserved lysine-362 in cytochrome *c* oxidase from *Rhodobacter sphaeroides*. *Biochemistry* **36**, 14456–14464 (1997).
36. D. Zaslavsky, R. B. Gennis, Proton pumping by cytochrome oxidase: Progress, problems and postulates. *Biochim. Biophys. Acta* **1458**, 164–179 (2000).
37. H.-M. Lee *et al.*, Mutations in the putative H-channel in the cytochrome *c* oxidase from *Rhodobacter sphaeroides* show that this channel is not important for proton conduction but reveal modulation of the properties of heme *a*. *Biochemistry* **39**, 2989–2996 (2000).
38. J. R. Fetter *et al.*, Possible proton relay pathways in cytochrome *c* oxidase. *Proc. Natl. Acad. Sci. U.S.A.* **92**, 1604–1608 (1995).
39. J. P. Hosler *et al.*, Polar residues in helix VIII of subunit I of cytochrome *c* oxidase influence the activity and the structure of the active site. *Biochemistry* **35**, 10776–10783 (1996).
40. M. L. Verkhovskaya *et al.*, Glutamic acid 286 in subunit I of cytochrome *bo*₃ is involved in proton translocation. *Proc. Natl. Acad. Sci. U.S.A.* **94**, 10128–10131 (1997).
41. S. Jünemann, B. Meunier, N. Fisher, P. R. Rich, Effects of mutation of the conserved glutamic acid-286 in subunit I of cytochrome *c* oxidase from *Rhodobacter sphaeroides*. *Biochemistry* **38**, 5248–5255 (1999).
42. B. Meunier, C. Ortwein, U. Brandt, P. R. Rich, Effects of mutation of residue I67 on redox-linked protonation processes in yeast cytochrome *c* oxidase. *Biochem. J.* **330**, 1197–1200 (1998).
43. A. Maréchal, B. Meunier, P. R. Rich, Assignment of the CO-sensitive carboxyl group in mitochondrial forms of cytochrome *c* oxidase using yeast mutants. *Biochim. Biophys. Acta* **1817**, 1921–1924 (2012).
44. A. Maréchal, A. M. Hartley, T. P. Warelow, B. Meunier, P. R. Rich, Comparison of redox and ligand-binding behaviour of yeast and bovine cytochrome *c* oxidases using FTIR spectroscopy. *Biochim. Biophys. Acta Bioenerg.* **1859**, 705–711 (2018).
45. L. Näsvik Öjemyr *et al.*, Reaction of wild-type and Glu243Asp variant yeast cytochrome *c* oxidase with O₂. *Biochim. Biophys. Acta* **1837**, 1012–1018 (2014).
46. M. L. Björck *et al.*, Proton-transfer pathways in the mitochondrial *S. cerevisiae* cytochrome *c* oxidase. *Sci. Rep.* **9**, 20207 (2019).

47. T. Tsukihara *et al.*, The low-spin heme of cytochrome *c* oxidase as the driving element of the proton-pumping process. *Proc. Natl. Acad. Sci. U.S.A.* **100**, 15304–15309 (2003).
48. K. Shimokata *et al.*, The proton pumping pathway of bovine heart cytochrome *c* oxidase. *Proc. Natl. Acad. Sci. U.S.A.* **104**, 4200–4205 (2007).
49. J. W. Thomas, A. Puustinen, J. O. Alben, R. B. Gennis, M. Wikström, Substitution of asparagine for aspartate-135 in subunit I of the cytochrome *bo* ubiquinol oxidase of *Escherichia coli* eliminates proton-pumping activity. *Biochemistry* **32**, 10923–10928 (1993).
50. U. Pfitzner *et al.*, Tracing the D-pathway in reconstituted site-directed mutants of cytochrome *c* oxidase from *Paracoccus denitrificans*. *Biochemistry* **39**, 6756–6762 (2000).
51. A. S. Pawate *et al.*, A mutation in subunit I of cytochrome oxidase from *Rhodobacter sphaeroides* results in an increase in steady-state activity but completely eliminates proton pumping. *Biochemistry* **41**, 13417–13423 (2002).
52. D. Han *et al.*, Replacing Asn207 by aspartate at the neck of the D channel in the aa_3 -type cytochrome *c* oxidase from *Rhodobacter sphaeroides* results in decoupling the proton pump. *Biochemistry* **45**, 14064–14074 (2006).
53. J. A. Garcia-Horsman, A. Puustinen, R. B. Gennis, M. Wikström, Proton transfer in cytochrome *bo3* ubiquinol oxidase of *Escherichia coli*: Second-site mutations in subunit I that restore proton pumping in the mutant Asp135→Asn. *Biochemistry* **34**, 4428–4433 (1995).
54. G. Brändén, A. S. Pawate, R. B. Gennis, P. Brzezinski, Controlled uncoupling and recoupling of proton pumping in cytochrome *c* oxidase. *Proc. Natl. Acad. Sci. U.S.A.* **103**, 317–322 (2006).
55. V. Rauhamäki, M. Wikström, The causes of reduced proton-pumping efficiency in type B and C respiratory heme-copper oxidases, and in some mutated variants of type A. *Biochim. Biophys. Acta* **1837**, 999–1003 (2014).
56. S. Yoshikawa *et al.*, Redox-coupled crystal structural changes in bovine heart cytochrome *c* oxidase. *Science* **280**, 1723–1729 (1998).
57. A. Shimada *et al.*, A nanosecond time-resolved XFEL analysis of structural changes associated with CO release from cytochrome *c* oxidase. *Sci. Adv.* **3**, e1603042 (2017).
58. I. Ishigami *et al.*, Crystal structure of CO-bound cytochrome *c* oxidase determined by serial femtosecond X-ray crystallography at room temperature. *Proc. Natl. Acad. Sci. U.S.A.* **114**, 8011–8016 (2017).
59. I. Ishigami *et al.*, Snapshot of an oxygen intermediate in the catalytic reaction of cytochrome *c* oxidase. *Proc. Natl. Acad. Sci. U.S.A.* **116**, 3572–3577 (2019).
60. A. Malkamäki, B. Meunier, M. Reidelbach, P. R. Rich, V. Sharma, The H channel is not a proton transfer path in yeast cytochrome *c* oxidase. *Biochim. Biophys. Acta Bioenerg.* **1860**, 717–723 (2019).
61. V. Sharma, P. G. Jambrina, M. Kaukonen, E. Rosta, P. R. Rich, Insights into functions of the H channel of cytochrome *c* oxidase from atomistic molecular dynamics simulations. *Proc. Natl. Acad. Sci. U.S.A.* **114**, E10339–E10348 (2017).
62. S. Supekar, A. P. Gamiz-Hernandez, V. R. I. Kaila, A protonated water cluster as a transient proton-loading site in cytochrome *c* oxidase. *Angew. Chem. Int. Ed. Engl.* **55**, 11940–11944 (2016).
63. J. Koepke *et al.*, High-resolution crystal structure of *Paracoccus denitrificans* cytochrome *c* oxidase: New insights into the active site and the proton transfer pathways. *Biochim. Biophys. Acta* **1787**, 635–645 (2009).
64. X. Cai *et al.*, Network analysis of a proposed exit pathway for protons to the P-side of cytochrome *c* oxidase. *Biochim. Biophys. Acta Bioenerg.* **1859**, 997–1005 (2018).
65. R. Sugitani, A. A. Stuchebrukhov, Molecular dynamics simulation of water in cytochrome *c* oxidase reveals two water exit pathways and the mechanism of transport. *Biochim. Biophys. Acta* **1787**, 1140–1150 (2009).
66. A. Maréchal, M. Iwaki, P. R. Rich, Structural changes in cytochrome *c* oxidase induced by binding of sodium and calcium ions: An ATR-FTIR study. *J. Am. Chem. Soc.* **135**, 5802–5807 (2013).
67. A. Timón-Gómez *et al.*, Mitochondrial cytochrome *c* oxidase biogenesis: Recent developments. *Semin. Cell Dev. Biol.* **76**, 163–178 (2018).
68. S. Riistama, L. Laakkonen, M. Wikström, M. I. Verkhovsky, A. Puustinen, The calcium-binding site in cytochrome aa_3 from *Paracoccus denitrificans*. *Biochemistry* **38**, 10670–10677 (1999).
69. B. Meunier, Site-directed mutations in the mitochondrially encoded subunits I and III of yeast cytochrome oxidase. *Biochem. J.* **354**, 407–412 (2001).
70. N. Fisher *et al.*, Human disease-related mutations in cytochrome *b* studied in yeast. *J. Biol. Chem.* **279**, 12951–12958 (2004).
71. J. Conde, G. R. Fink, A mutant of *Saccharomyces cerevisiae* defective for nuclear fusion. *Proc. Natl. Acad. Sci. U.S.A.* **73**, 3651–3655 (1976).
72. B. J. Thomas, R. Rothstein, Elevated recombination rates in transcriptionally active DNA. *Cell* **56**, 619–630 (1989).
73. B. Guérin, P. Labbe, M. Somlo, Preparation of yeast mitochondria (*Saccharomyces cerevisiae*) with good P/O and respiratory control ratios. *Methods Enzymol.* **55**, 149–159 (1979).